Experimental Investigation of Circumferential Inlet Distortion on Partial Surge Type Stall Inception in Transonic Axial Compressor *

YAN Jian-dong[1], PAN Tian-yu[2,3,4], WU Wen-qian[1], LI Qiu-shi[2,3,5]

(1. School of Energy and Power Engineering, Beihang University, Beijing 100191, China;
2. National Key Laboratory of Science and Technology on Aero-Engine Aero-Thermodynamics, Beihang University, Beijing 100191, China;
3. Research Institute of Aero-Engine, Beihang University, Beijing 100191, China;
4. Advanced Jet Propulsion Creativity Center, Aero Engine Academy of China, Beijing 101300, China;
5. Key Laboratory of Fluid and Power Machinery, Xihua University, Chengdu 610039, China)

Abstract: To explore the mechanism of stall point shift in detail, a series of experiments are conducted to explore the effects of circumferential inlet distortions on compressor instability evolutions with three different distortion intensities. During the experiments, the high-response dynamic test points are mounted to measure static pressures at rotor tips and total pressures at stator trailing edges, and an additional test point is set on the wall of the plenum to detect the system response. The results demonstrate that the decrease of mass flow rate near rotating stall under circumferential inlet distortions is due to that it is the occurrence of spike-type stall inception that leads to the flow instability instead of that of the partial surge. The instability inception of partial surge occurs under uniform inlet conditions and it is in the form of axisymmetric low-frequency disturbances localized in the stator hub region. The low-frequency disturbance still can appear under circumferential inlet distortions but the propagation characteristic of axisymmetric is suppressed. Therefore, the low-frequency disturbance cannot be further developed, and the final compressor instability is caused by the spike-type inception at the rotor tip. In conclusion, circumferential inlet distortion can change the stall route so as to extend the stalled operation point.

Key words: Transonic axial compressor; Stall margin; Stall inception; Circumferential inlet distortion; Partial surge

CLC number: V235.1 **Document code**: A **Article number**: 1001-4055 (2023) 01-210804-11

DOI: 10.13675/j.cnki. tjjs. 210804

实验探究周向进气畸变对局部喘振型跨声速轴流压气机进气的影响

闫建东[1]，潘天宇[2,3,4]，武文倩[1]，李秋实[2,3,5]

（1. 北京航空航天大学 能源与动力学院，北京 100191；
2. 北京航空航天大学 航空发动机气动热力学国家重点实验室，北京 100191；

* **收稿日期**：2021-11-17；**修订日期**：2022-01-14。

基金项目：国家自然科学基金（51976005；52006002）；国家科技重大专项（2017-II-0005-0018）；航空发动机及燃气轮机基础科学中心项目（P2022-B-II-004-001）；先进航空动力创新工作站（HKCX2020-02-013）；中央高校基本科研业务费专项资金；北京市科技新星计划。

作者简介：闫建东，博士生，研究领域为压气机稳定性。

通讯作者：潘天宇，博士，副教授，研究领域为压气机稳定性、气动弹性。E-mail：pantianyu@buaa.edu.cn

引用格式：闫建东，潘天宇，武文倩，等．实验探究周向进气畸变对局部喘振型跨声速轴流压气机进气的影响[J]．推进技术，2023，44(1)：210804．（YAN Jian-dong, PAN Tian-yu, WU Wen-qian, et al. Experimental Investigation of Circumferential Inlet Distortion on Partial Surge Type Stall Inception in Transonic Axial Compressor [J]. *Journal of Propulsion Technology*, 2023, 44(1): 210804.）

3. 北京航空航天大学 航空发动机研究院，北京 100191；
4. 先进航空动力创新工作站 中国航空发动机研究院，北京 101300；
5. 西华大学 流体与动力机械重点实验室，四川 成都 610039）

摘 要：为深入探究失速点变化机理，采用实验方法探究了三种不同周向畸变强度的进气边界对压气机失稳演化的影响机理。在试验过程中，通过增加动态测试点以测量转子叶尖的静压和静子尾缘的总压，并在压气机出口容腔内增加测点以检测系统响应。结果表明，当进口存在周向畸变时，失稳点流量的减小是由于压气机的失稳演化过程从局部喘振转变成了突尖波。在均匀进气时，该压气机失速演化过程为局部喘振，扰动以低频轴对称的形式出现在静子叶根区域。当进口存在周向畸变时，静子叶根处仍会出现不稳定低频扰动，但由于周向畸变的存在使其不再具备轴对称性，因此该低频扰动无法进一步发展，最终由于转子叶尖出现了突尖波导致压气机失稳。本研究主要结论为周向进气畸变可以通过改变压气机失速过程进而影响压气机失速点变化。

关键词：跨声速压气机；稳定裕度；失速先兆；周向进气畸变；局部喘振

1 Introduction

The uniform inflow is not always realised at the inlet section during application. When the engine encounters the distortion inflow, the compressor has the potential to rotating stall or surge, which can lead to catastrophic consequences. Thus, the investigation of inlet distortion has been implemented since the 1950s due to practical problems, like gust, ground swirl, and flight maneuvers [1]. The previous experimental studies suggest that the inlet distortion deteriorates the compressor performance and reduces the stall margin (increase in stall mass flow) in most circumstances[2-7]. Due to the limitations of the instrument, only steady-state data can be measured in previous experiments. As for the simulation method, Mazzawy [8] and Hynes et al[9] built two-dimensional simulation models to investigate the propagation of small-amplitude disturbances under the circumferential inlet distortion condition. The computation capability at that time, however, was not sufficient, so their models inevitably made some assumptions. Therefore, the physical mechanisms of the reduction in stall margin have not been fully understood for five decades. As for applications in engineering, the compressor designers usually sacrifice operation range to ensure the compressor can tolerate transient distortion inflow.

Until recently, to fulfill the economic target, the boundary layer ingestion (BLI) ideal was proposed in 2009[10]. The BLI aircraft configuration has great potential in reducing noise and fuel consumption. The circumferential distortion has become a continuous operating condition for the modern compressor design. Therefore, the requirements for compressor stability under continuous circumferential distortion conditions have been proposed immediately. Circumferential distortion has become a subject of increasing interest in compressor stability over recent years. With improved measurement methods in experiments, the cycling behaviour of the unsteady disturbance under circumferential inlet distortion (in some cases BLI distortion) was reported by many researchers experimentally[11-13]. The disturbances at the rotor tip grow in the low-momentum area and decay in the high-momentum area, which is related to the swirl angle and mass flow distribution. The compressors stall when the disturbance can propagate around the annular without dying out in the high-momentum region. Specifically, the total pressure distortion at the tip dominates the variation of the incidence angle so as to affect the propagation of disturbance. It has also been found, by means of that computational method, that the circumferential inlet distortion has a non-negligible influence on the compressor stability. Fidalgo et al.[14] illustrate the formation of the swirl flow upstream of the rotor. They found that the reduction in stall margin linearly increases with the distortion intensity. Zhang et al.[15] compared the distortion in different ranges and found that the greatest distortion range leads to a more considerable loss in the stall margin. The adverse effect of circumferential distortion in this research is illustrated by the flow blockage at the blade tip. Wenqiang et al. studied the circumferential distortion simulation systematically, including the computation model, boundary conditions, physical timesteps, and exit duct length [16-18]. One interesting finding is that the length of the exit duct is an important feature to be considered if one wants to simulate the stall margin of a compressor with circumferential distortion. Those investigations mainly focus on spike-type stall inception compressors. The spike-type stall inception is a short-length-scale disturbance originating from the rotor tip within serval pitches in width. The formation of the spike is related to the three-dimensional flow at the tip[19-21]. Therefore, the compressor with spike-type stall inception also is classified as tip critical compressor as the unstable phenomena occur in the rotor tip region first.

Recently, various new stall inceptions have been developed, focusing largely on hub highly load. This increases the possibility of instability in the flow at the hub. Dodds et al.[22-23] found stall cells at the rotor hub rotating at a relatively low speed. Pan et al.[24-27] reported a partial surge in 2014 and further investigated it in the after years. The low-frequency partial surge disturbance originates from the stator hub with no circumferential phase difference. The influence of circumferential inlet distortion on the hub critical compressor remains unclear. The subject of this paper is to reveal the influence of circumferent inlet distortion on a transonic axial compressor with partial surge stall inception. Different intensities of circumferent inlet distortion are implemented experimentally.

2 Experimental methods

2.1 Compressor rig and measurement system

A schematic view of the test equipment is presented in Fig. 1. A power turbine drives the tested compressor, connecting by a gearbox. The rotation speed can increase continuously to the maximum value of 24000 r/min. Experiments in this paper were all tested at 88% design speed (around 19360 r/min) because, in our previous studies, the partial surge typically causes the stall inception when running at 88% design speed. The torque meter is connected to the gearbox to measure the total work input. The setting chamber eliminates the non-uniform inflow from the environment and guarantees similar inlet flow conditions before the gauze. Thus, the gauze is mounted downstream of the chamber. The test rig is a single-stage transonic compressor. The specification of the compressor is summarised in Table 1 and Table 2.

To illustrate the measurement system on the tested compressor, the tested stage configuration is shown in Fig. 2. The circumferential inlet distortion is introduced by installing a distortion gauze sector at the compressor's intake downstream of the settling chamber. The parameters of the gauze are well-designed and summarised in Table 3. The d and l represent the wire diameter and interval distance, respectively. Low-response total pressure probes are located at the inlet (Sections A) and outlet (Section D) of the compressor. Specifically, six combs are used to get the total pressure accurately at the outlet section under a highly skewed total pressure transversal distribution. There are five measurement positions at each comb equal-area distributed along the radial direction. The total pressures are averaged by the area-average method. The steady-state total pressure probes are 24PC produced by Honeywell, which the full-scale output error is within 0.25%. Four high-respondent static pressure transducers are mounted upstream of the rotor leading edge equal-circumferential distance (Section B). Downstream of the stator, twelve dynamic total pressure transducers are mounted at an equal distance from each other in the circumferential and radial direction. To monitor the pressure in the plenum downstream of the compressor outlet, static pressure transducers are mounted in the plenum. The dynamic total pressure and static pressure transducers are Kulite XL-140-20D and Kulite XL-190-25D, in which the full-scale output errors are within 0.05% and 0.1%.

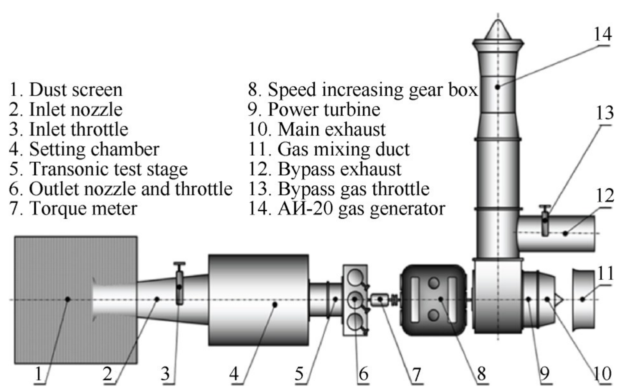

Fig. 1 Schematic diagram of the rig test facility

Table 1 Design parameters of the compressor

Parameter	Value
Rotor speed/(r/min)	2.2×10^4
Total pressure ratio	1.6
Design mass flow rate/(kg/s)	13.5
Hub/Tip ratio of rotor	0.565
Aspect ratio of rotor	0.956
Number of rotor blade	17
Number of stator blade	29
Number of splitter blade	29

Table 2 Detailed blade parameters

Parameter	Inflow angle/(°)	Outflow angle/(°)	Solidity
Rotor tip	61.7	61.7	1.29
Rotor middle	58.55	50.89	1.54
Rotor hub	49.1	10.1	2.09
Stator tip	47.02	23.00	1.36
Stator middle	44.27	23.94	1.52
Stator hub	53.35	32.83	1.81
Splitter tip	23.00	−7.86	0.94
Splitter middle	27.89	−5.04	1.13
Splitter hub	34.39	−7.37	1.33

2.2 Data acquisition and analysis

In this paper, three different gauzes are mounted upstream of the rotor. For quantification of the distortion intensities, the distortion coefficient definition is given below[28]

Table 3 Design parameters of gauzes

Distortion intensity (DC_{120})	d/m	l/m
0.33	0.10	0.35
0.47	0.09	0.25
0.52	0.08	0.18

$$DC_{120}=\frac{p_{\text{Average}}-p_{\text{Distorted}}}{\frac{1}{2}\rho v^2} \tag{1}$$

To acquire the operation condition and compressor performance, the measurement system records for over five seconds at each steady-state operation point. The data in the compressor map is averaged by more than 50 samples to smooth the environment noise. The mass flow is calculated by

$$\dot{m}=\kappa_m\cdot K\frac{p_0^*\pi R^2}{\sqrt{T_0^*}}q(\lambda_0) \tag{2}$$

κ_m is a boundary layer correlation coefficient. K is an aerodynamic coefficient, 0.0404. p_0^*, T_0^* is total pressure and temperature downstream the setting chamber. R is the radius of the probe. $q(\lambda_0)$ is an aerodynamic parameter calculated from the inlet total pressure temperature and static pressure.

For the total pressure measurement, there are four combs mounted at the inlet section, assuming that there is not much mixing right after the gauze. Two combs are set in the distorted region, and the other two are placed in the undistorted region. The total pressure counter at the outlet section could be very complex, so six combs

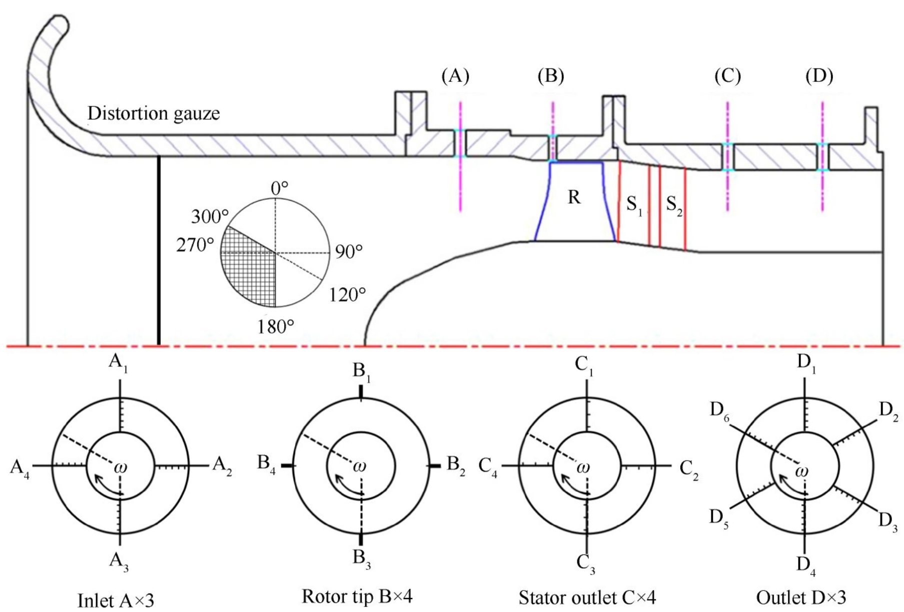

Fig. 2 Tested stage and configuration of measurement system

are mounted at cross-section D. All the data recorded is area-averaged to obtain the total pressure value at each section. The total pressure ratio is defined by

$$\pi^* = \frac{p_{\mathrm{out}}^*}{p_{\mathrm{in}}^*} \tag{3}$$

Adiabatic torque efficiency is used in this paper.

$$\eta = \frac{m \cdot \dfrac{kR}{k-1} \cdot T_{\mathrm{t,in}} \cdot \left[\left(\pi_{\mathrm{r}}^* \right)^{\frac{k-1}{k}} - 1 \right]}{\left(g \cdot T_{\mathrm{t,in}} \right) \cdot \left(\dfrac{2\pi}{60} n \right)} \tag{4}$$

$T_{\mathrm{t,in}}$ is the torque input measured by the torque meter as presented in Fig. 1.

The high-response measurement system is activated around the near stall operation point in the uniform inflow case. The near stall operation point was estimated based on previous experiments. In the distortion case, the high-response measurement system is activated after the peak total pressure ratio point. The sampling frequency of this high-response measurement system is 50 kHz. All the dynamic data is appropriately filtered to show the stall event in the next chapter.

3 Experimental results

The overall compressor performance and the instability evolution with different inflow conditions are demonstrated in this section. In particular, the pre-stall behaviours with uniform and distorted inflow are shown for comparison.

3.1 Overall performances

In Fig. 3, uniform total-to-total pressure ratio (*TPR*) and efficiency are plotted against distortion inflows. The results were obtained under the same thermal conditions. The pressure ratio and efficiency in the inlet distortion cases are lower compared with the uniform case throughout the whole operating range, showing that the distortion has an adverse effect on the compressor performance.

Among those three distortion cases with different intensities, the change of stall point mass flow is consistent with the findings in other papers. As the distortion intensity rises, the stall point mass flow rate increases. This observation has led others to posit that an increase in distortion intensity causes a greater total pressure difference between the distorted and undistorted regions. Therefore, both the axial velocity and swirl angle have changed. After the gauze, the axial velocity is reduced, and the enlarged circumferential heterogeneity produces a stronger swirl angle at the edge of distortion. The spikes stall inception is related to the incidence angle. At the trailing edge of the distortion region, the incidence reaches its maximum value around the annular. As a result, the stronger intensity of distortion, the larger the stall point mass flow rate is. Because the stall inception has converted from partial surge to spikes, this explanation also applies to this compressor.

However, an unexpected result shows that the stall point mass flow rates of the three circumferential distortions cases decrease by 6.7%~8.7% when compared with the uniform case, instead of increasing or remaining the same value as reported in other papers. Thus, the following chapters discuss the stall events to investigate the reduction of the stall point mass flow rate.

3.2 Instability evolution

The rig was throttled slightly from the final stable operation point during the distortion cases to trigger the whole compressor instability. The evolutions of stall processes recorded by dynamic measurement and steady

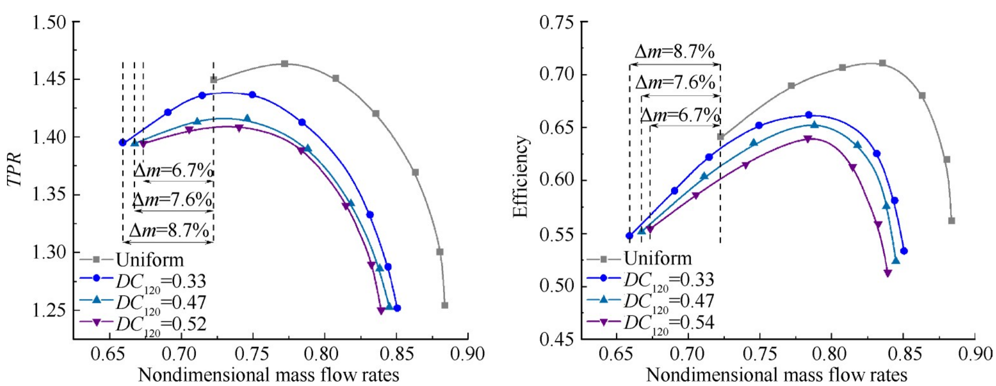

Fig. 3 Compressor performances

measurement are analysed to reveal the mass flow rate reduction mechanism.

The stall inception of this compressor at 88% design speed is the typical partial surge, as indicated by previous studies [24-27], originating in the stator hub region. Thus, the stator hub total pressure data from all four cases are processed by the windows Fourier transform (WFT) method in Fig. 4. Note that the timeframes of all four cases are rearranged by defining the stall point as the 0th revolution to show the relative chronological order of the low and high-frequency disturbances. Low-frequency disturbances are marked by light grey stripes, and high-frequency disturbances are marked by dark grey stripes. In the uniform case, the partial surge disturbances occur axis-symmetrically around 250 revolutions prior to the stall point. In the distortion cases, however, the low-frequency disturbances become unsynchronised between distorted and undistorted regions. It is shown that the circumferential distortion has an adverse effect on the stability in the distorted region. As a result, the flow in the distorted region tends to become unstable prior to the distorted region, as marked by the blue surfaces. To further investigate the stall event in the distortion cases, more analyses on the distortion case with DC_{120}=0.33 are presented in the following section.

Fig.5 shows the normalised pressure coefficient at the stator hub in the uniform case and distortion case with DC_{120}=0.33. Hereafter, the circumferential distortion case refers to the circumferential distortion with DC_{120}=0.33, unless specifically stated. The normalised pressure coefficient is calculated as the total pressure value divided by the maximum total pressure value, aiming to show the relative amplitude of the disturbances compared to the surge. In the uniform case, the stalled process is divided into two periods: the hub margin and

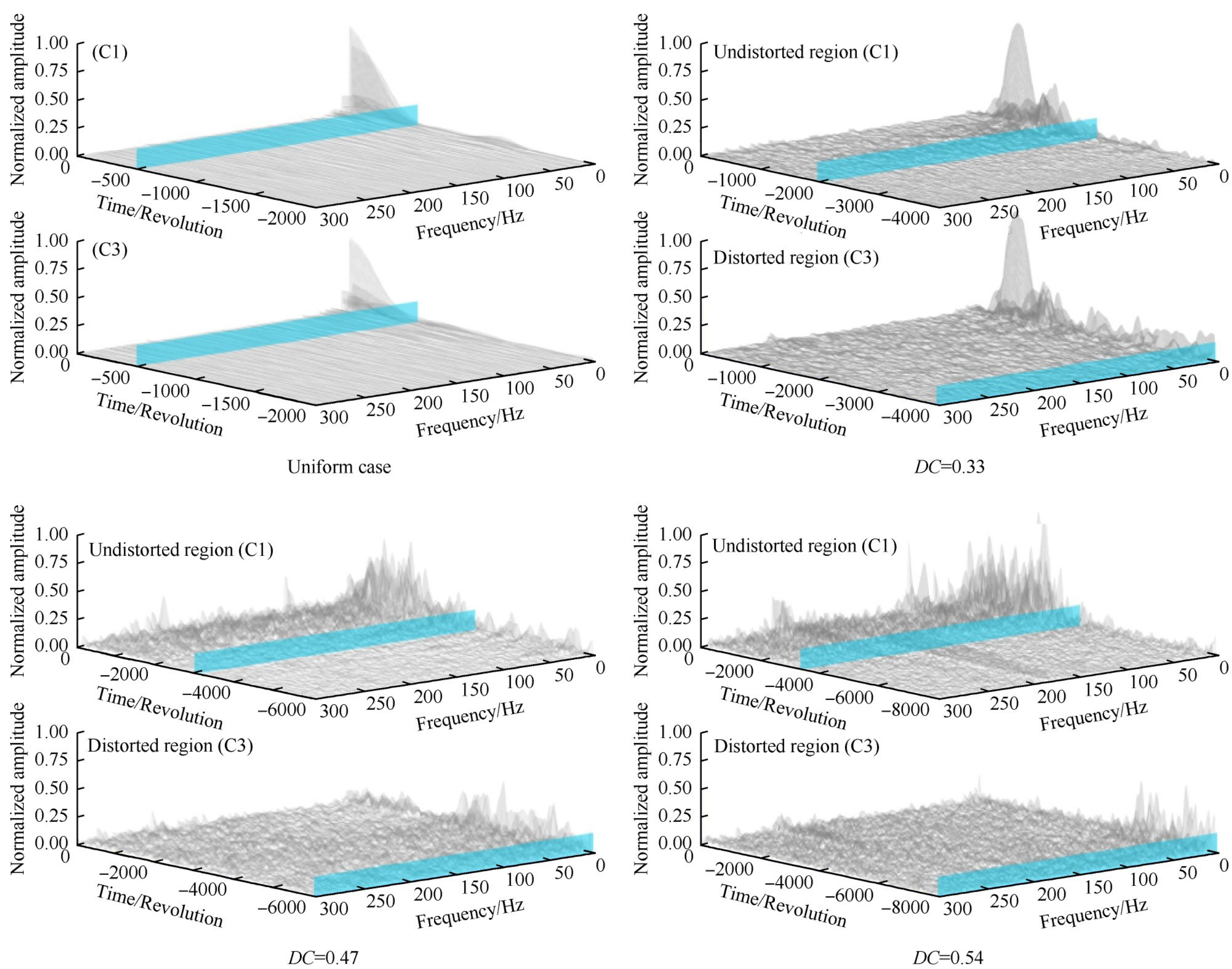

Fig. 4 WFT results of the data from the stator hub in uniform and three circumferential distortion cases

the partial surge, distinguished by grey dash lines. Some small-scale disturbances occur in the stator hub region before the occurrence of the partial surge, indicating that the flow in the stator hub region has become unstable. At 250 revolutions prior to the stall point, continuous partial surge disturbances occur. The fluctuations of total pressure lead to the variation of the incidence angle. With a decreased mass flow rate, namely the axial velocity, the incidence angle exceeds the critical value and the compressor stall with rotating stall cells.

The whole stall event of the circumferential distortion case is introduced in three periods: the hub margin, the partial surge, and the tip margin, each distinguished by grey dash lines. Note that the distorted and undistorted are plotted in black and blue, respectively. The low-frequency disturbances occur at the −1900th revolution in the undistorted region. Then, those low-frequency disturbances become more and more frequent. The amplitude of those disturbances is almost twice as large as the value in the uniform case and is of the same magnitude as the partial surge disturbances. In the circumferential direction, those low-frequency disturbances are not synchronous between the distorted region and the undistorted region. It is not until the 1420th revolution that some downward disturbances occur in the distorted hub region, indicating that the flow in the distorted region has become unsteady. Those disturbances, however, are with smaller amplitudes compared with the value in the undistorted region.

After 150 revolutions, the continuous partial surge disturbances occur with two downward pulses. The continuous partial surge disturbances last for 660 revolutions and convert from high-level total pressure with downward pulses to low-level total pressure with upward pulses. Those disturbances are axisymmetric at the stator hub as there is no phase difference between distorted and undistorted regions. It is shown that the circumferential distortion has little effect on the partial surge disturbance in the hub region. Without leading to the whole compressor instability, the continuous partial surge disturbances disappear at around −400th revolution.

Following the −400th revolution, there are no significant unsteady flow phenomena observed on this scale until the stall point. During this period, the unsteady phenomena localise at the rotor tip in the form of high-frequency, small-amplitude disturbances, which will be demonstrated later.

The low-frequency disturbance in the undistorted region is related to the circumferential distortion as

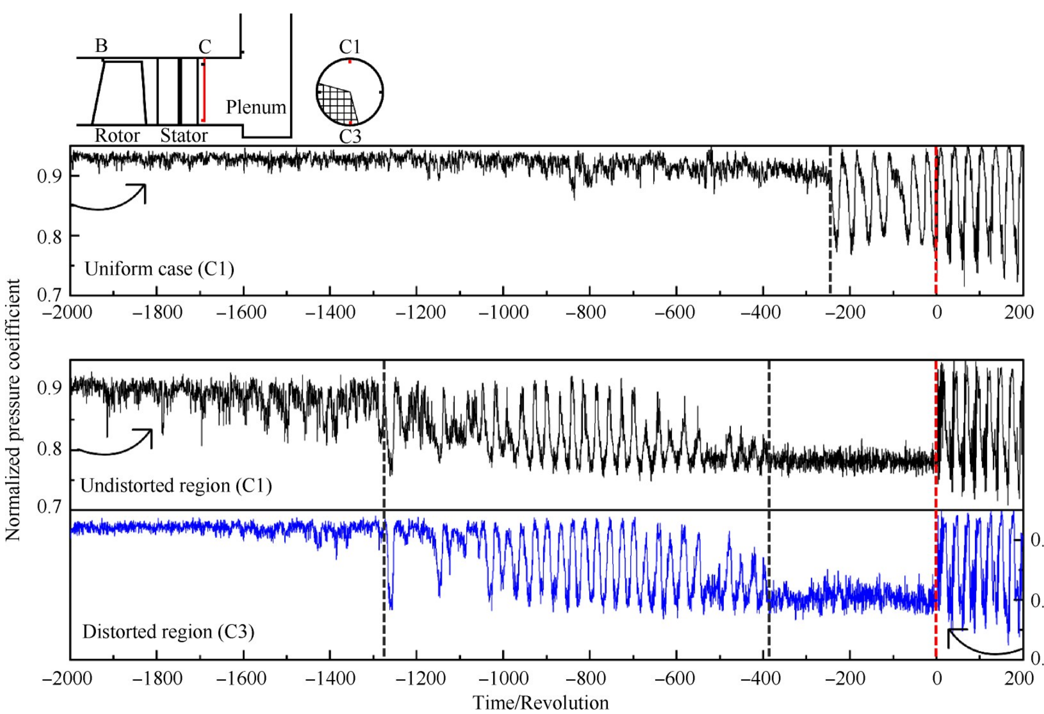

Fig. 5 Pressure signal in different positions from the uniform and DC_{120}=0.33 cases

those disturbances only localise a portion of the hub region. Thus, to further demonstrate the features of those disturbances, the data from rotor tip, stator tip, stator hub and plenum during the hub margin period are replotted in Fig. 6. There are corresponding disturbances in the stator tip region for those low-frequency disturbances in the stator hub region. Unlike the continuous partial disturbances, however, those disturbances have little effect on the rotor tip and plenum. The amplitude of the disturbance indicates that the disturbances originate in the stator hub and can only propagate radially. The frequency of those disturbances is around 7Hz from the FFT result, smaller than the Helmholtz frequency, showing that this disturbance is different from the partial surge disturbance. Based on our previous experiments, several downward pulses could occur before the continuous partial surge disturbances, which also occurs in this experiment. However, the low-frequency disturbances, in this case, originate in only a portion of the annular over varying frequencies compared to the partial surge disturbance. Thus, it is a reasonable hypothesis that the low-frequency disturbance is relative to the circumferential distortion. The circumferential distortion loads a portion of the hub region. Therefore, in the highly loaded region, the flow tends to become unstable early. This can also be verified from the WFT results in Fig. 4, where the low-frequency always occurs early in the undistorted region, considering all the three distortion cases.

After 150 revolutions, partial surge disturbances occur. It is axisymmetric in the hub region, as plotted in Fig. 7. The spectral analysis on the right shows that the frequency of the partial surge is still 12Hz, which is identical to the previous result in the uniform inflow case. However, unlike the uniform case, the continuous partial surge disturbances fail to induce the formation of rotating stall cells.

To further explain this result, the WFT results from the four transducers tapped on the rotor casing wall are shown in Fig. 8 to show both the continuous partial surge disturbance and the high-frequency disturbance. The partial surge disturbance in the undistorted region is larger than that of the distorted region at the rotor tip. Thus, the high-frequency disturbance associated with the partial surge disturbance rise in the undistorted region, as denoted by the black arrow, and stays at the ground value in the distorted region, denoted by the blue arrow. The relationship between the partial surge disturbance and high-frequency disturbance was explained in 2017 by Pan et al.[29]. The high-frequency

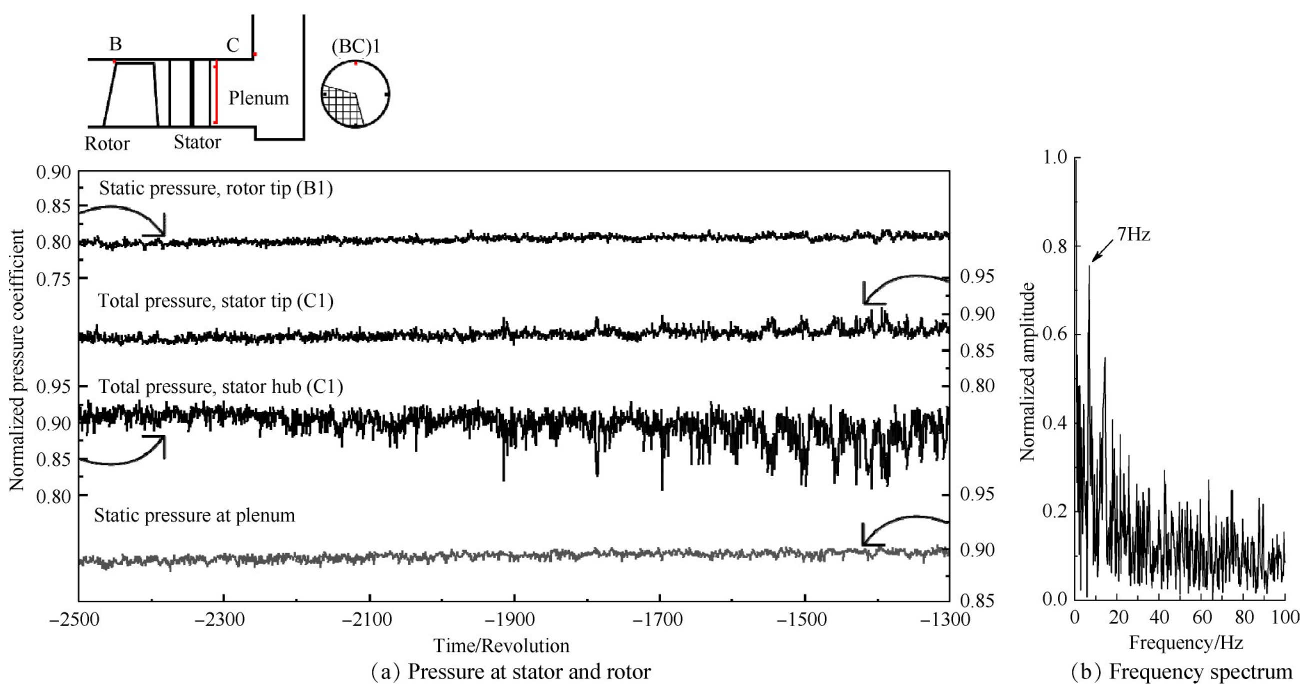

(a) Pressure at stator and rotor (b) Frequency spectrum

Fig. 6 Disturbances during the hub margin period

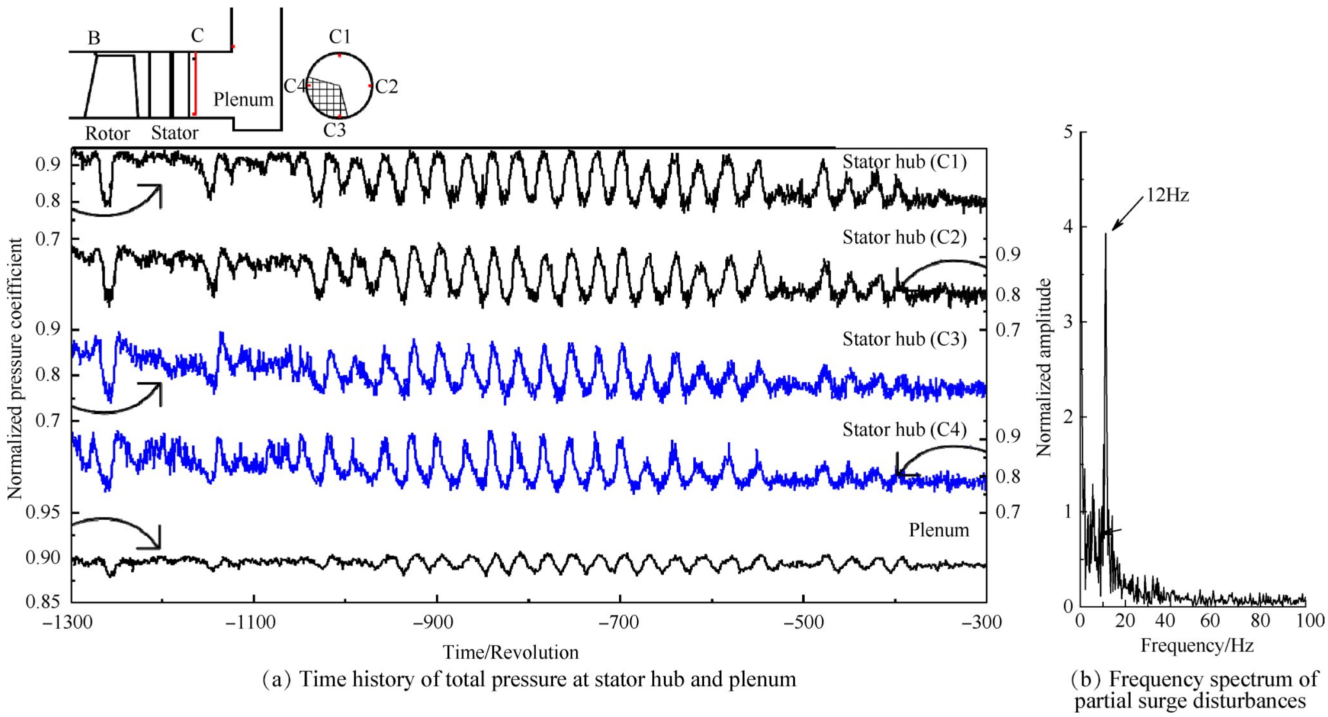

(a) Time history of total pressure at stator hub and plenum

(b) Frequency spectrum of partial surge disturbances

Fig. 7　Characteristics of partial surge

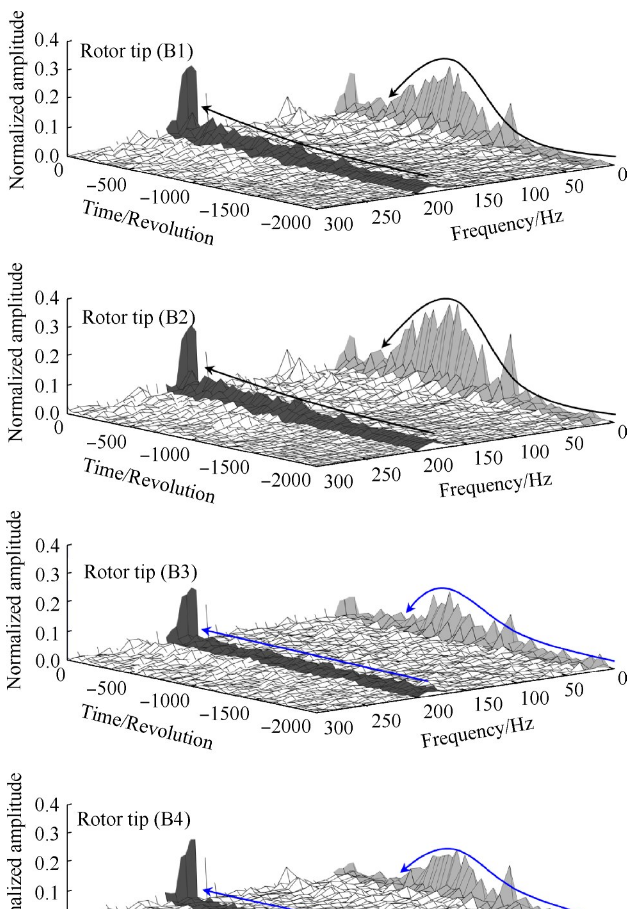

Fig. 8　WFT results of the data from the rotor tip to show the partial surge disturbance and high-frequency disturbance

disturbance, namely the unformed rotating stall cell disturbance, fails to propagate around the annular. As a result, the compressor can still operate steadily during the partial surge disturbance period.

After the disappearance of the partial surge, no significant unsteady flow phenomena on a large scale occurs until the stall point. This is because the unsteady disturbances are localised in the rotor region on smaller scales. Thus, the pressure data from the rotor tip is filtered by the high-frequency pass method and plotted in Fig. 9. Black dash lines mark that the high-frequency disturbances appear in the undistorted region and disappear in the distorted region until the spike occurs in the distorted region.

With further throttled, the high-frequency disturbance in the distorted region begins to rise. When the blade exits the distortion region, its loading reaches its maximum in the distortion region. A downward spike type stall inception occurs, marked in the red circle in Fig. 9, and the rotating stall cells form and propagate along the annular. This is then followed by spikes. The initial speed of spike propagation speed is around 0.65 rotor pass frequency (RPF) and decreases to 0.57 RPF with the final formation of stall cells.

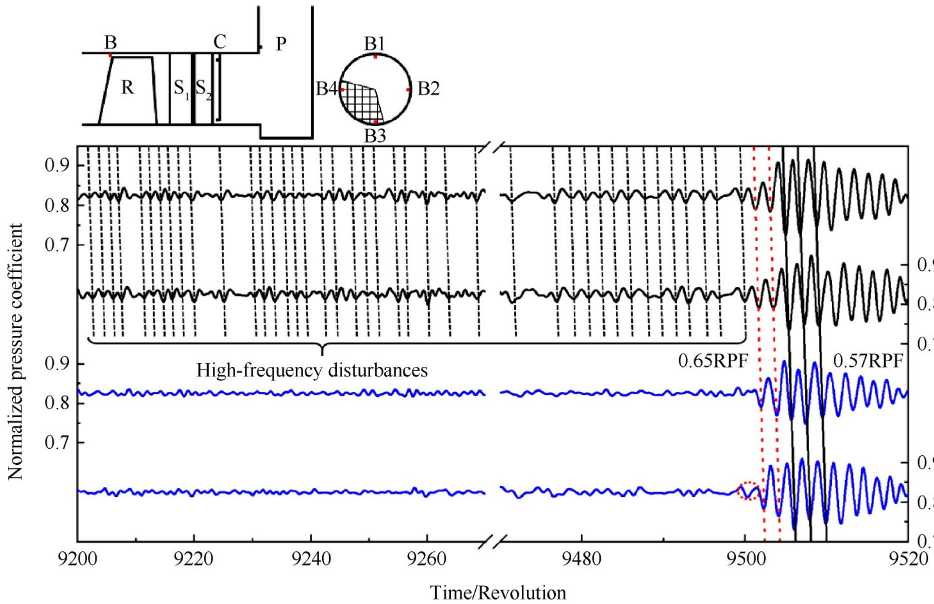

Fig. 9 Schematic to demonstrate the stall inception evolution

4 Conclusions

The effects of circumferential distortion on partial-surge stall inception are demonstrated on a transonic compressor in this paper. The instability evolutions with uniform and distortion inflow are in the investigation. Unlike other tip-critical compressors, the experimental results show that the stalled point mass flow rate is not adversely affected by distortion. The experimental data are analysed to show the difference in instability evolution. Under the circumferential distortion, the stall inception that triggers the whole compressor instability is converted from partial surge to spikes. The unsteady phenomenon before the stall still suggests that the flow of the stator hub region has the potential to become unstable and grow into large-amplitude disturbances. Two different routes that lead to stall are presented. The key findings are as follow:

(1) The circumferential distortion can reduce the stalled point mass flow rate by converting the partial surge inception into spikes inception. This is highlighted by comparison with the uniform case.

(2) In the DC_{120}=0.33 distortion case, the distortion mainly influences the tip region. At the tip, the amplitude of the partial surge disturbance is much lower than in the distorted area. Thus, the high-frequency disturbances associated with the partial surge disturbances in the distorted area are below the critical value and fail to propagate into rotating stall cells.

Acknowledgement: The authors acknowledge the support of the National Natural Science Foundation of China ; National Science and Technology Major Project ;Science Center for Gas Turbine Project ; Advanced Jet Propulsion Creativity Center; the Fundamental Research Funds for the Central Universities, and Beijing Nova Program.

References

[1] Conrad E W, Sobolewski A E. Investigation of Effects of Inlet-Air Velocity Distortion on Performance of Turbojet Engine[R]. *Technical Report Archive & Image Library*, 1950.

[2] Ehrich F. Circumferential Inlet Distortions in Axial Flow Turbomachinery [J]. *Journal of the Aeronautical Sciences*, 1957, 24(6): 413-417.

[3] Katz R. Performance of Axial Compressors with Asymmetric Inlet Flows[D]. *California*: *Institute of Technology*, 1958.

[4] Doyle M D C, Horlock J H. Circumferential Asymmetry in Axial Flow Compressors[J]. *The Journal of the Royal Aeronautical Society*, 1966, 70(670): 953-957.

[5] Plourde G A, Stenning A H. Attenuation of Circumferential Inlet Distortion in Multistage Axial Compressors[J]. *Journal of Aircraft*, 1968, 5(3): 236-242.

[6] Biesiadny T J, Braithwaite W M, Soeder R H, et al. Summary of Investigations of Engine Response to Distorted Inlet Conditions[C]. *Munich*: *The* 68*th Meeting of the Propulsion and Energetic Panel*, 1986.

[7] Jaumotte A L. The Influence of Flow Distortions on Axial Flow Fan and on Rotating Stall[J]. *Journal of Applied*

Mathematics and Physics, 1964, 15: 116-125.

[8] Mazzawy R S. Multiple Segment Parallel Compressor Model for Circumferential Flow Distortion[J]. *Journal of Engineering for Gas Turbines and Power*, 1977, 99(2): 288-296.

[9] Hynes T P, Greitzer E M. A Method for Assessing Effects of Circumferential Flow Distortion on Compressor Stability [J]. *Journal of Turbomachinery*, 1987, 109 (3): 371-379.

[10] Hall C A, Schwartz E, Hileman J I. Assessment of Technologies for the Silent Aircraft Initiative[J]. *Journal of Propulsion and Power*, 2009, 25(6): 1153-1162.

[11] Siggeirsson E M V, Andersson N, Olander M B. Numerical and Experimental Aerodynamic Investigation of an S-Shaped Intermediate Compressor Duct with Bleed[R]. *ASME GT* 2020-15336.

[12] Jiang Huabing, Lu Yajun, Yuan Wei, et al. Experimental Investigation of the Influence of Inlet Distortion on the Stall Inception in a Low Speed Axial Compressor[R]. *ASME GT* 2009-59139.

[13] Perovic D, Hall C A, Gunn E J. Stall Inception in a Boundary Layer Ingesting Fan[J]. *Journal of Turbomachinery*, 2019, 141(9): 1-10.

[14] Fidalgo V J, Hall C A, Colin Y. A Study of Fan-Distortion Interaction Within the NASA Rotor 67 Transonic Stage[J]. *Journal of Turbomachinery*, 2012, 134 (5): 1-12.

[15] Zhang H, An K, Tan F, et al. Numerical Investigation of Effect of Inlet Distortion on Compressor Flow Field and Stability[R]. *ASME GT* 2017-63369.

[16] Zhang W, Stapelfeldt S, Vahdati M. Influence of the Inlet Distortion on Fan Stall Margin at Different Rotational Speeds[J]. *Aerospace Science and Technology*, 2019, 98: 105668.

[17] Zhang W, Vahdati M. A Parametric Study of the Effects of Inlet Distortion on Fan Aerodynamic Stability [J]. *Journal of Turbomachinery*, 2019, 141(1): 1-15.

[18] Zhang W, Vahdati M. Influence of the Inlet Distortion on Fan Stall Margin at Different Rotational Speed [C]. *Shanghai*: *The 30th Global Power and Propulsion*, *GPPS*-2017-0207.

[19] Furukawa M, Inoue M, Saiki K, et al. The Role of Tip Leakage Vortex Breakdown in Compressor Rotor Aerodynamics[J]. *American Society of Mechanical Engineers*, 1999, 239: 469-480.

[20] Vo H D, Tan C S, Greitzer E M. Criteria for Spike Initiated Rotating Stall[J]. *Journal of Turbomachinery*, 2008, 130(1): 155-165.

[21] Pullan G, Young A M, Day I J, et al. Origins and Structure of Spike-Type Rotating Stall[J]. *Journal of Turbomachinery*, 2015, 137(5): 051007.

[22] Dodds J, Vahdati M. Rotating Stall Observations in a High Speed Compressor—Part I: Experimental Study[J]. *Journal of Turbomachinery*, 2015, 137(5): 1-9.

[23] Dodds J, Vahdati M. Rotating Stall Observations in a High Speed Compressor—Part II: Numerical Study[J]. *Journal of Turbomachinery*, 2015, 137(5): 1-9.

[24] Pan Tianyu, Yan Zhaoqi, Sun Dakun, et al. Effect of System Response on Partial Surge Initiated Instability in a Transonic Axial Flow Compressor[J]. *Chinese Journal of Aeronautics*, 2022, 35(2): 117-127.

[25] Pan Tianyu, Li Qiushi, Li Zhiping, et al. Effects of Radial Loading Distribution on Partial-Surge-Initiated Instability in a Transonic Axial Flow Compressor[J]. *Journal of Turbomachinery*, 2017, 139(10): 1470-1479.

[26] Li Qiushi, Pan Tianyu, Li Zhiping, et al. Experimental Study of Compressor Instability Inception in a Transonic Axial Flow Compressor[R]. *ASME GT* 2014-25190.

[27] Li Qiushi, Pan Tianyu, Sun Tailu, et al. Experimental Investigations on Instability Evolution in a Transonic Compressor at Different Rotor Speeds[J]. *Journal of Mechanical Engineering Science*, 2015, 229(18): 3378-3391.

[28] Reid C. The Response of Axial Flow Compressors to Intake Flow Distortion[C]. *Cleveland*: *ASME* 1969 *Gas Turbine Conference and Products Show*, 1969.

[29] Pan Tianyu, Li Qiushi, Yuan Wei, et al. Effects of Axisymmetric Arc-Shaped Slot Casing Treatment on Partial Surge Initiated Instability in a Transonic Axial Flow Compressor[J] *Aerospace Science and Technology*, 2017, 69: 257-268.

（编辑：刘萝威）